Journal of Biomolecular NMR **27:** 261–275, 2003.

Characterization of the overall and local dynamics of a protein with intermediate rotational anisotropy: Differentiating between conformational exchange and anisotropic diffusion in the B3 domain of protein G

Jennifer B. Hall & David Fushman*
Department of Chemistry and Biochemistry, Center for Biomolecular Structure and Organization, University of Maryland, College Park, MD 20742, U.S.A.

Received 19 February 2003; Accepted 5 May 2003

Key words: anisotropic rotational diffusion, conformational exchange, CSA/dipolar cross-correlation, hydrodynamic calculations, immunoglobulin-binding domain, protein dynamics, protein G

Abstract

Because the overall tumbling provides a major contribution to protein spectral densities measured in solution, the choice of a proper model for this motion is critical for accurate analysis of protein dynamics. Here we study the overall and backbone dynamics of the B3 domain of protein G using ^{15}N relaxation measurements and show that the picture of local motions is markedly dependent on the model of overall tumbling. The main difference is in the interpretation of the elevated R_2 values in the α-helix: the isotropic model results in conformational exchange throughout the entire helix, whereas no exchange is predicted by anisotropic models that place the longitudinal axis of diffusion tensor almost parallel to the helix axis. Due to small size (fast tumbling) of the protein, the T_1 values have low sensitivity to NH bond orientation. The diffusion tensor derived from orientation dependence of R_2/R_1 is anisotropic ($D_{par}/D_{perp} = 1.4$), with a small rhombic component. In order to distinguish the correct picture of motion, we apply model-independent methods that are sensitive to conformational exchange and do not require knowledge of protein structure or assumptions about its dynamics. A comparison of the CSA/dipolar cross-correlation rate constants with ^{15}N relaxation rates and the estimation of R_{ex} terms from relaxation data at 9.4 and 14.1 T indicate no conformational exchange in the helix, in support of the anisotropic models. The experimentally derived diffusion tensor is in excellent agreement with theoretical predictions from hydrodynamic calculations; a detailed comparison with various hydrodynamic models revealed optimal parameters for hydrodynamic calculations.

Introduction

Nuclear spin-relaxation parameters contain a multitude of information about the overall and local mobility of polypeptides (e.g., Palmer et al., 1996; Palmer, 1997; Fushman and Cowburn, 1998b). Fast internal protein dynamics which occur in a ps-ns time range (i.e. molecular bond reorientations and dihedral angle fluctuations) are usually characterized by squared order parameters (S^2) and local correlation times (τ_{loc}) that can be derived from measured ^{15}N relaxation rates (typically, R_1, R_2, NOE) using the 'model-free' approach (Lipari and Szabo, 1982). Conformational exchange on a slower, μs-ms time scale can be also determined (e.g., Clore et al., 1990a; Szyperski et al., 1993; Orekhov et al., 1994; Akke and Palmer, 1996; Ishima et al., 1998; Loria et al., 1999). Superimposed on these local dynamics is the overall tumbling of protein molecule in solution – due to restricted amplitudes and short correlation times of local motions, the overall rotation could be the dominant contribution to the measured values of R_1 and R_2.

*To whom correspondence should be addressed. E-mail: fushman@wam.umd.edu

In order to obtain an accurate picture of protein dynamics, the contributions from local motions must be correctly deconvolved from those originating from the overall tumbling. This deconvolution is severely complicated if the rotational diffusion of a molecule is not isotropic. The case of anisotropic rotational diffusion seems to be quite general for proteins and reflects deviation in the shape of the molecule from a perfect sphere. In this case the ^{15}N spin relaxation rates depend on the orientation of the backbone amide N-H vectors with respect to the principal axes frame of the rotational diffusion tensor. The microdynamic parameters derived from these data could be in error if the rotational anisotropy is not taken into account (as pointed out in e.g., Schurr et al., 1994; Fushman and Cowburn, 1998b). Specifically, it has been shown (Tjandra et al., 1996b; Luginbuhl et al., 1997; Fushman and Cowburn, 1998b) that an analysis which does not include rotational anisotropy could result in spurious conformational exchange motions. Accurate identification of these motions in a protein is of particular interest in view of their potential relevance to biological function (e.g., Eisenmesser et al., 2002).

Therefore development of robust procedures for relaxation data analysis in the presence of rotational anisotropy is of considerable importance for protein dynamics studies. Several approaches have been developed recently in order to derive the overall rotational diffusion tensor from the orientation dependence of the spin-relaxation rates (Tjandra et al., 1995; Lee et al., 1997; Copie et al., 1998; Blackledge et al., 1998; Fushman et al., 1999b; Dosset et al., 2000; Ghose et al., 2001). This information can then be used to improve the accuracy of the microdynamic parameters derived from the relaxation data.

When anisotropy of the overall rotational diffusion is significant, the conventional protocol for deriving local dynamic parameters in the case of isotropic overall tumbling (Kay et al., 1989; Farrow et al., 1994; Mandel et al., 1995; Fushman et al., 1997) is no longer sufficient, and a model-free analysis must be modified to take into account the anisotropy of the overall rotation. For large anisotropy, characterized by a ratio of the principal components of the diffusion tensor $D_{||}/D_{\perp} \geqslant 2$, this has long been accepted. For small anisotropy ($D_{||}/D_{\perp} = 1.17$) it has been shown that the model-free parameters obtained assuming anisotropic overall tumbling are not significantly different from those derived using the isotropic model (Tjandra et al., 1995). The effect of overall anisotropy on relaxation parameters increases approximately linearly with $(D_{||}/D_{\perp}) - 1$ (Fushman and Cowburn, 1998b; Fushman et al., 1999b) so it is significant already in the case of intermediate anisotropy and therefore could be mistaken for conformational exchange. Our analysis of a representative set of 878 protein structures suggests that about 70% of monomeric proteins have $1.2 < D_{||}/D_{\perp} < 2$ (Geraghty et al., unpublished).

Here we use ^{15}N relaxation measurements to study the overall and local dynamics in the B3 domain of protein G, further called GB3, a small protein with intermediate rotational anisotropy ($D_{||}/D_{\perp} \approx 1.4$). We apply several methods, some of which rely upon and some of which are independent of the knowledge of protein structure or assumptions about protein dynamics, to differentiate between conformational exchange and the overall rotational anisotropy, in order to distinguish the correct picture of motion. The derived diffusion tensor is then compared with the results of hydrodynamic models to determine proper parameters for the hydrodynamic calculations.

Materials and methods

The GB3 domain construct in these studies comprised 56 amino acids: The residue numbers 1 through 56 used here correspond to residues 6–61 in the sequence used in the crystal structure (Derrick and Wigley, 1994). The unstructured five-residue long N-terminal fragment was clipped off. Also, the first two residues, Thr^6 and Thr^7, in the native sequence of the construct were mutated to Met^1 and Gln^2.

The protein sample for NMR studies contained 1.8 mM of uniformly ^{15}N enriched protein dissolved in 30 mM phosphate buffer (pH 5.8) containing 9% D_2O. The protein was a generous gift from Dr. Ad Bax. The experiments were performed on a Bruker DRX spectrometer operating at ^{1}H resonance frequency of 600.13 MHz (field 14.1 Tesla). Sample temperature was set to 24 °C. Relaxation measurements include rates of ^{15}N longitudinal (R_1) and transverse (R_2) relaxation and the rate of ^{15}N-^{1}H cross-relaxation measured via steady-state ^{15}N{^{1}H} nuclear Overhauser effect (NOE). The experiments used standard pulse sequences described elsewhere (Fushman et al., 1997). Relaxation-compensated CPMG measurements utilized the approach suggested in (Loria et al., 1999); the repetition delays between successive ^{15}N 180° pulses were set to 1 ms, 4 ms, and 8 ms. The steady-state heteronuclear ^{15}N{^{1}H} NOEs were determined using water flip-back measurement

scheme (Grzesiek and Bax, 1993), the recycling delay was 5.5 s. In addition, R_1, R_2, and hetero-NOE were also measured at 9.4 Tesla (400 MHz) on a Bruker AVANCE 400 spectrometer (CERM, University of Florence).

To minimize temperature variations between the spectra acquired with different relaxation delays and to minimize the effect of possible sample instability during a series of measurements, the experiments were performed in an interleaved fashion, as a pseudo-3D experiment with the 2D planes in the F2 dimension corresponding to various relaxation delays. The acquisition order (3-2-1) was designed so that cycling through various relaxation delays (in R_1 or R_2 experiments) or through NOE/NONOE 2D planes was performed prior to incrementing the evolution period in the indirect dimension (F1). Five 2D planes were recorded for each relaxation rate measurement, following the optimal sampling strategy (Jones, 1997). The relaxation delays were 8 ms and 264 ms ($\times$4) for R_2 and 4 ms and 440 ms ($\times$4) for R_1 measurements. The recycling delay was typically set to 3.2 s for R_2 and 1.7 s for R_1. Relaxation rates were derived by fitting the observed cross peak intensities in a series of 2D planes to a mono-exponential decay. Experimental errors in peak intensities were estimated by integrating regions of spectra containing no cross peaks.

The transverse ^{15}N CSA-dipolar cross-correlation rates (η_{xy}) were measured using the method of (Tjandra et al., 1996a) with relaxation delays 2Δ set to 63.82, 85.10, 106.38 and 127.64 ms, and from a direct analysis of differential transverse relaxation of the ^{15}N doublet in a series of ^{1}H-coupled ^{1}H-^{15}N HSQC-type spectra with different durations (63.82, 85.10, and 95.74 ms) of the constant-time evolution period that also served as the relaxation period (Hall et al., 2003). The signal overlap problem of coupled HSQC spectra was addressed by implementing an IPAP scheme (Ottiger et al., 1998); the IP and AP experiments were run in an interleaved fashion, as a pseudo-3D experiment.

The measurements of longitudinal ^{15}N CSA-dipolar cross-correlation rates (η_z), were based on the method of (Kroenke et al., 1998). The η_z values were obtained using a variant of the original pulse sequence and then uniformly scaled by a correction factor derived from separate η_z measurements based on direct analysis of differential longitudinal relaxation of the ^{15}N doublet components in ^{1}H-coupled ^{1}H-^{15}N HSQC-type spectra (J.B. Hall and D. Fushman, in preparation). The duration of the active relaxation delay was set to 100, 200, 300 and 400 ms.

All spectra were processed using XWINNMR (Bruker Instruments). Further analysis including automatic peak picking and integration, relaxation curve fitting and data analysis was performed using an in-house suite of Matlab programs PICK, RELAXFIT, DYNAMICS (Fushman et al., 1997), R2R1 (Fushman et al., 1999b), ETAFIT, and ROTDIFF.

The rotational diffusion tensor for anisotropic models was derived directly from the ratio of the measured values of R_2 and R_1, as outlined earlier (Fushman et al., 1999b), using only those residues that belong to the well-defined core of the protein and excluding Gln^2 which is a mutation. These calculations were performed using program ROTDIFF (Walker et al., in preparation). The characteristics of the diffusion tensor were then used as input into the program DYNAMICS (Fushman et al., 1997) to obtain model-free parameters for each amide group. The DYNAMICS program has been modified to handle the case of full anisotropy.

Results and discussion

Preliminary analysis of the hydrodynamic properties of the protein

The protein used as a model for this analysis is the B3 immunoglobulin-binding domain of streptococcal protein G (Gronenborn et al., 1991; Achari et al., 1992; Derrick and Wigley, 1992; Derrick et al., 1993; Gallagher et al., 1994). The structure of the GB3 domain has been solved by both X-ray crystallography (Derrick and Wigley, 1994) and NMR (Lian et al., 1992) and shows a well-packed hydrophobic core formed by a four-stranded β-sheet and a four-turn α-helix (Figure 1).

The inertia tensor of the protein was calculated using the coordinates of the heavy atoms from the crystal structure (1IDG). It has the ratio of the principal values of 1.80:1.79:1.00, indicating that the protein can be modeled as an axially symmetric rotor. The unique axis of the tensor is approximately parallel to the α-helix axis as shown in Figure 1.

A rough theoretical estimate of the principal components, D_i ($i = x, y,$ or z), of the diffusion tensor and of the overall correlation time, τ_c, of GB3 can be made assuming Stokes–Einstein–Debye hydrodynamics model in which the protein is approximated as a rigid rotor in the shape of a cylinder or prolate ellipsoid and using empirical relationships from the

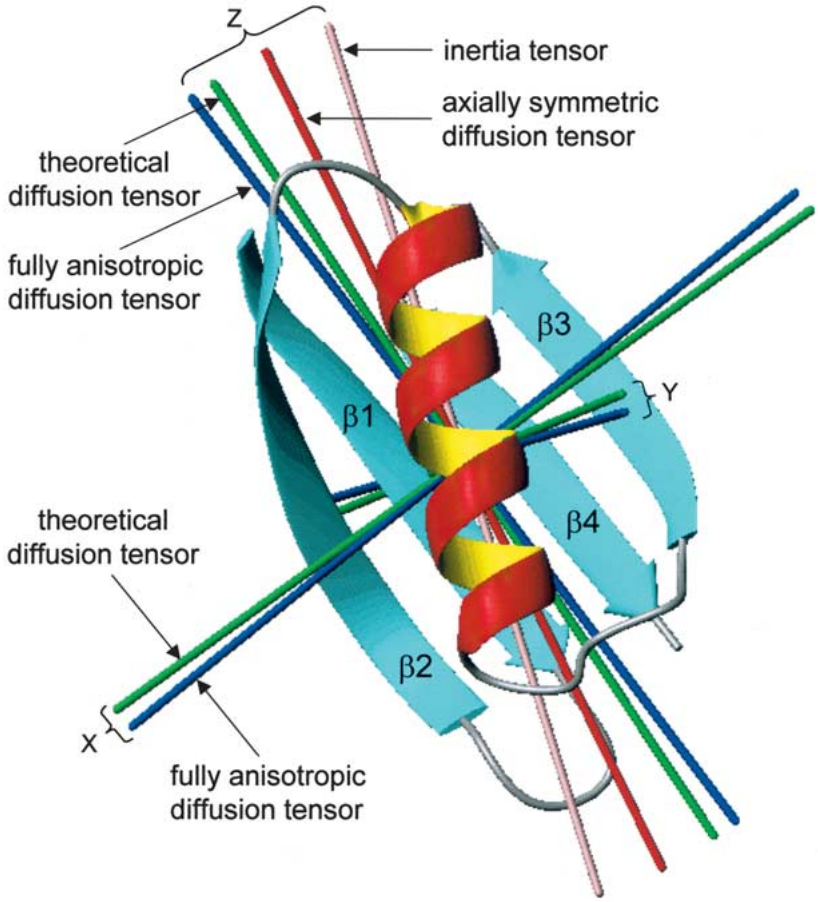

Figure 1. Cartoon representation of the tertiary structure of the GB3 domain (56 a.a.), generated using MolMol (Koradi et al., 1996). Various rods represent the orientation of the diffusion tensor axes (as indicated) obtained directly from ^{15}N relaxation data for the axially symmetric (red) and fully anisotropic (blue) models and predicted theoretically (green) using HYDRONMR, along with the unique axis of the inertia tensor (pink). Atom coordinates are from the crystal structure (1IDG) (Derrick and Wigley, 1994). The orientations of all three diffusion tensors are similar within the experimental errors. The z-axis of the axially symmetric tensor makes an 8° angle with those for the fully anisotropic tensors, both measured and predicted using HYDRONMR. The difference in the orientation of the z-axes of the fully anisotropic and the theoretical tensor is 3°. All these z-axes are oriented approximately along the α-helix axis: the tilt angle is 23°, 30° and 28°, for the axially symmetric, fully anistotropic, and the HYDRONMR-predicted tensors. Similar angles with respect to the unique axis of the inertia tensor are 10°, 18° and 17°; this axis is tilted from the helix axis by 15°.

literature (Tirado and de la Torre, 1980). The cylinder approximation resulted in $D_{||}/D_{\perp} = 1.45$ and $\tau_c = 2.35$ ns, assuming solvent viscosity of 0.91 cpoise at 24 °C. The sizes of the molecule in the relevant dimensions (27 Å in the z and 16 Å in both x and y, the axial ratio 1.69) were obtained from the crystal structure. The axial ratio for the cylinder estimated from the inertia tensor values is 1.64.

For a prolate ellipsoid model, the ratio of the principal values of the diffusion tensor is approximately given by $D_{||}/D_{\perp} \approx (I_{\perp}/I_{||})^{1/\sqrt{2}}$ (Copie et al., 1998), where $I_{||}$ and $I_{\perp}$ are the principal components of the inertia tensor. Using this simple hydrodynamics model, we obtained $D_{||}/D_{\perp} = 1.51$ and $\tau_c = 2.64$ ns under identical solvent conditions.

Based on these data, one could anticipate anisotropic overall tumbling of the molecule with the diffusion tensor axis oriented approximately parallel to the α-helix axis (Figure 1). All these estimations do not include a hydration shell, the effects of which are explored later, along with a discussion of more sophisticated hydrodynamics models.

The ^{15}N relaxation data

55 resolved backbone amide cross peaks were observed in the 2D spectra. Though they could be suf-

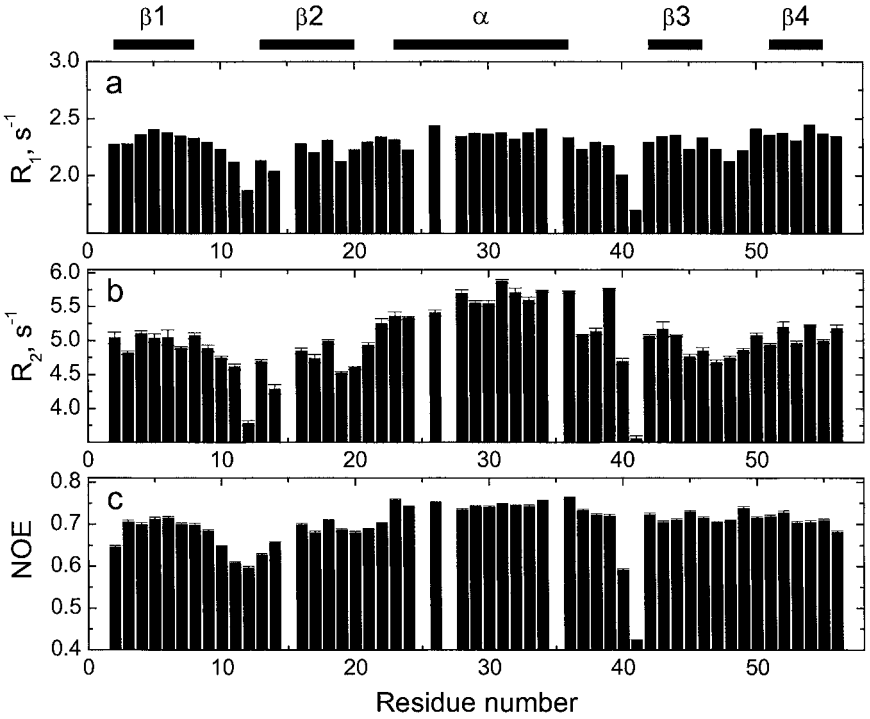

Figure 2. Amide ^{15}N relaxation rates at 14.1 Tesla, (a) R_1, (b) R_2, and (c) ^{15}N{^{1}H} NOE versus residue number for the B3 domain of protein G. The error bars represent standard errors in the experimental parameters. The horizontal bars on the top indicate the positions of the secondary structure elements in the protein sequence.

Table 1. Hydrodynamic characteristics of the GB3 domain derived from ^{15}N relaxation data using various models of the overall tumbling and from hydrodynamics calculations

Model of overall motion	D_x^a	D_y^a	D_z^a	Θ^b	Φ^b	Ψ^b	τ_c^c	Anisotropy[d]	Rhombicity[e]	χ^2/df[f]	P[g]
Isotropic	4.86 (0.04)	4.86 (0.04)	4.86 (0.04)	–	–	–	3.43 (0.03)	1	0	102.5	–
Axial symmetry	4.45 (0.11)	4.45 (0.11)	6.07 (0.33)	69 (12)	94 (7)	–	3.34 (0.11)	1.37 (0.06)	0	8.4	4×10^{-17}
Full anisotropy	4.13 (0.24)	4.60 (0.18)	6.25 (0.34)	68 (7)	85 (10)	179 (14)	3.34 (0.10)	1.43 (0.09)	0.37 (0.24)	6.2	5×10^{-3}
Theoretical prediction[h]	4.43	4.64	6.36	64	87	175	3.31	1.40	0.17		

Numbers in the parentheses represent standard deviations.
[a]Principal values (in 10^7 s^{-1}) of the rotational diffusion tensor, ordered so that $D_x \leq D_y \leq D_z$.
[b]Euler angles $\{\Phi, \Theta, \Psi\}$ (in degrees) describe the orientation of the principal axes frame of the rotational diffusion tensor with respect to protein coordinate frame.
[c]Overall rotational correlation time (in ns) of the molecule, $\tau_c = 1/[2\ Tr(\underline{\underline{D}})]$.
[d]The degree of anisotropy of the diffusion tensor, $2D_z/(D_x + D_y)$.
[e]The rhombicity of the diffusion tensor, $1.5(D_y - D_x)/[D_z - \frac{1}{2}(D_x + D_y)]$.
[f]Residuals of the fit (χ^2) divided by the number of degrees of freedom.
[g]Probability that the reduction in χ^2 (compared to the model in the row directly above it) could occur by chance. Both axially symmetric and fully anisotropic models are statistically a much better fit than the isotropic model.
[h]The results of hydrodynamic calculations using HYDRONMR program (García de la Torre et al., 2000); parameter a was set to 2.6 Å.

ficiently resolved for assignment, residues Glu[15] and Asn[35] and Thr[25] and Glu[27] are not included in relaxation analysis as their signal intensities could be affected by spectral overlap. Gln[2] was excluded from anisotropic analyses because it is not present in the available protein coordinates. The relaxation paramet-

ers for the GB3 domain are presented in Figure 2. The R_1, R_2 and NOE data show simultaneous decrease in the β1/β2 loop and between the α-helix and β3 strand, thus indicating flexible regions in the protein. There is no such decrease in any of the relaxation parameters in the region between β2 and the α-helix, however, and between strands β3 and β4 there is a decrease in R_1 and R_2 but not in the NOE.

Noticeably elevated R_2 values are observed for the entire α-helix (Figure 2b). The NOEs here are also somewhat higher than in the rest of the backbone, while the R_1 values are at about same level as or slightly higher than in the other elements of the secondary structure. An elevation in R_2 of the magnitude observed in the α-helix is usually indicative of conformational exchange on the microsecond-millisecond timescale, and similar values in the B1 domain of protein G have been ascribed to conformational exchange caused by minor rotational motion of the α-helix relative to the β-sheet that curls around it (Barchi et al., 1994). However, given the structure of GB3, it is difficult to imagine a physical model that would account for every residue in the helix (including those not facing the β-sheet) being involved in conformational exchange. The analysis of (Barchi et al., 1994) was based on the isotropic model for the overall tumbling. An alternative interpretation was proposed in (Tillett et al., 2000) for similar behavior of R_2s observed in the B2 domain of protein G. Their analysis based on the axially symmetric tumbling model suggests that there is no conformational exchange in the α-helix. Given the differences in the outcome of these analyses for the related B1 and B2 domains of protein G, it is of significant interest to determine the correct picture of motions in the GB3 domain.

The orientational dependence of the transverse relaxation rate could account for the elevation in R_2 for residues in the α-helix if the helix axis of the GB3 domain is aligned parallel to the longitudinal axis of the prolate rotational diffusion tensor. This orientation will align the NH vectors in the α-helix along the axis of fast overall rotation – as the result, they will experience slower rates of overall tumbling (hence higher R_2s) compared to the rest of the protein. However, since the transverse and longitudinal relaxation rates have an opposite dependence on the orientation of N-H vectors with respect to the diffusion tensor axis, a concomitant decrease in the R_1 values would typically be expected for the amides in the α-helix. Such a decrease is not observed in GB3 (Figure 2a). In order to resolve this apparent contradiction, we determined the overall rotational diffusion tensor of GB3 using the ^{15}N relaxation data.

Characterization of the rotational diffusion tensor of the protein from ^{15}N relaxation data

The rotational diffusion tensor of the protein was derived from the orientation dependence of $(2R'_2/R'_1 - 1)^{-1}$ as described in (Fushman et al., 1999b); the primes here indicate that the relaxation rates were modified to subtract the contributions from high-frequency components of the spectral density (Fushman et al., 1999a). Only those residues belonging to well-defined elements of the secondary structure were used in this analysis. Residues in the flexible loops and in the termini, where the N-H bond orientation might not be well defined, were not included. Note that the diffusion tensor derived by this method is independent, to the first order approximation, from the values of the order parameter and from the site-specific variations in the ^{15}N CSA (Fushman, 2002; Fushman and Cowburn, 2002). The characteristics of the rotational diffusion tensor of GB3 derived using various models are presented in Table 1.

For the axially symmetric model, the rotational diffusion tensor of GB3 is characterized by $D_{||}/D_{\perp} = 1.37 \pm 0.06$ and $\tau_c = 3.34 \pm 0.11$ ns. The orientation of its unique principal axis with respect to the crystal structure (Figure 1) is characterized by $\Theta = 69° \pm 12°$, $\Phi = 94° \pm 7°$. This model agrees with the experimental data significantly better than the isotropic model: the F-statistics analysis of the fit results in the probability $P = 5 \times 10^{-17}$ that this could occur by chance. A small angle between the axis of the diffusion tensor and the α-helix axis (Figure 1) would then explain the observed elevated R_2 values in this part of the protein.

The characteristics of the diffusion tensor derived assuming full anisotropy are very similar (Table 1, Figure 1). These data suggest that GB3 tumbling in solution is not perfectly axially symmetric, which is also supported by the results of hydrodynamic calculations (below). The full anisotropy model provides an improvement in the fit over the axially symmetric model, with the confidence level of 99.5% ($P = 0.005$). This improvement, however, is not as dramatic as when going from isotropic to axially symmetric model. Therefore, for completeness, we will keep both anisotropic models (axially symmetric and fully anisotropic) in further analysis.

Note that the overall rotational correlation time (3.34 ns) derived here is in good agreement with 3.3 ns reported in (Barchi et al., 1994) for a similar-length B1 domain construct (at 26 °C). Somewhat higher values of τ_c (3.69 ns) and rotational anisotropy (1.68) observed in the B2 domain (Tillett et al., 2000) (at 27 °C) are likely due to longer (64 a.a.) construct and its more elongated shape because of the flexible N- and C-termini.

Microdynamic parameters: Three models of overall motion

The backbone microdynamic parameters (S^2, τ_{loc}) and R_{ex} contributions (if any) were determined for GB3 using the following three models of the overall rotational diffusion tensor: Isotropic, axially symmetric, and fully anisotropic. The overall correlation time for the isotropic model was optimized simultaneously with the model-free analysis (see Fushman et al., 1997). The characteristics of the rotational diffusion tensor for anisotropic models were derived as described in the previous section and then used to obtain residue-specific values of the microdynamic parameters (see Materials and methods). Values for S^2 and R_{ex} for each residue are shown in Figure 3.

All three models show simultaneous decrease in the order parameters in the β1/β2 loop and in the loop between the α-helix and β3 indicating particularly flexible regions. In the region between β2 and the α-helix, and in the β3/β4 loop there is a small decrease in order parameter, indicating that these regions are more flexible than the elements of secondary structure but less flexible than the other, more extended loops. All three models show elevated order parameters in the region of the α-helix. The fully anisotropic and axially symmetric models predict slightly higher values for the order parameters in this region than does the isotropic model (see insert). For most of the NH groups, the order parameters derived using the two anisotropic models are practically indistinguishable from each other; the exceptions are Leu^{12}, Gly^{41}, Asp^{47} and Ala^{48} located in the flexible loops as well as Ala^{20} and Asp^{36} at the very edge of the β2 strand and the α-helix, respectively. Excluding Ala^{20} and Asp^{36} from the list of protein core residues for the fully anisotropic diffusion tensor analysis results in a 24% reduction in the χ^2 of the fit while the values of the derived parameters (e.g., $D_{||}/D_{\perp}$, τ_c, etc.) stay within their respective confidence limits. If these values are then used to calculate order parameters, there is no perceptible change except for $Ala^{20}$and Asp^{36} where the agreement between the axially symmetric and fully anisotropic models is significantly improved.

The values of local correlation time (not shown) derived from these analyses varied from 0 to 56 ps for the majority of backbone amides, except for those (16 residues for the isotropic and 8 and 9 for axially and fully anisotropic diffusion tensors) where the extended model-free approach (Clore et al., 1990b) was required. In the latter case, the correlation time for slow motions varied from 0.80 to 3.56 ns.

The most striking difference between the isotropic and anisotropic models is in the resulting maps of conformational exchange motions (Figure 3b–d). The isotropic model predicts conformational exchange in a stretch of 13 residues, Glu^{24}, Lys^{28}-Ala^{34}, and Asp^{36}-Asp^{40}, covering the entire α-helix (note that Thr^{25}, Glu^{27}, and Asn^{35} were excluded due to signal overlap), while a significantly lesser number of sites show this type of motion when rotational anisotropy is taken into account. Only for Val^{39} do all three models agree, making it a likely candidate for conformational exchange. However, the value of R_{ex} for this residue (0.78 s^{-1}, 0.51 s^{-1} and 0.28 s^{-1} for the isotropic, axially-symmetric and fully anisotropic models, respectively) seems to depend heavily on the model of overall motion. Both the axial and fully anisotropic models (but not the isotropic model) suggest R_{ex} contributions for Lys^{13}, and Glu^{56}. Note that Val^{39} is located in the middle of a flexible α/β3 loop, Lys^{13} is at the end of a flexible loop β1/β2, and Glu^{56} is the C-terminal residue. The orientation of the NH vector for these residues might not be well defined, so the predicted R_{ex} values could reflect a particular NH bond orientation in the crystal structure rather than a real conformational exchange motion. To determine if such a bias due to orientation in the crystal structure exists, we performed similar analysis using a bundle of 24 NMR structures of GB3 (PDB file 2IGH) (Lian et al., 1992). For all these structures, a fully anisotropic model predicted conformational exchange for Val^{39}, indicating that these motions are likely to be real (see also below). No R_{ex} contribution was found in Glu^{56} for any of the 24 NMR structures, so the conformational exchange predicted for this residue was probably due to bias. R_{ex} terms (although small, less than 0.2 s^{-1}) were obtained for Lys^{13} in 16 out of the 24 NMR structures. This suggests that the predicted conformational exchange for Lys^{13} is not likely to be due to bias caused by the use of the (single) crystal structure.

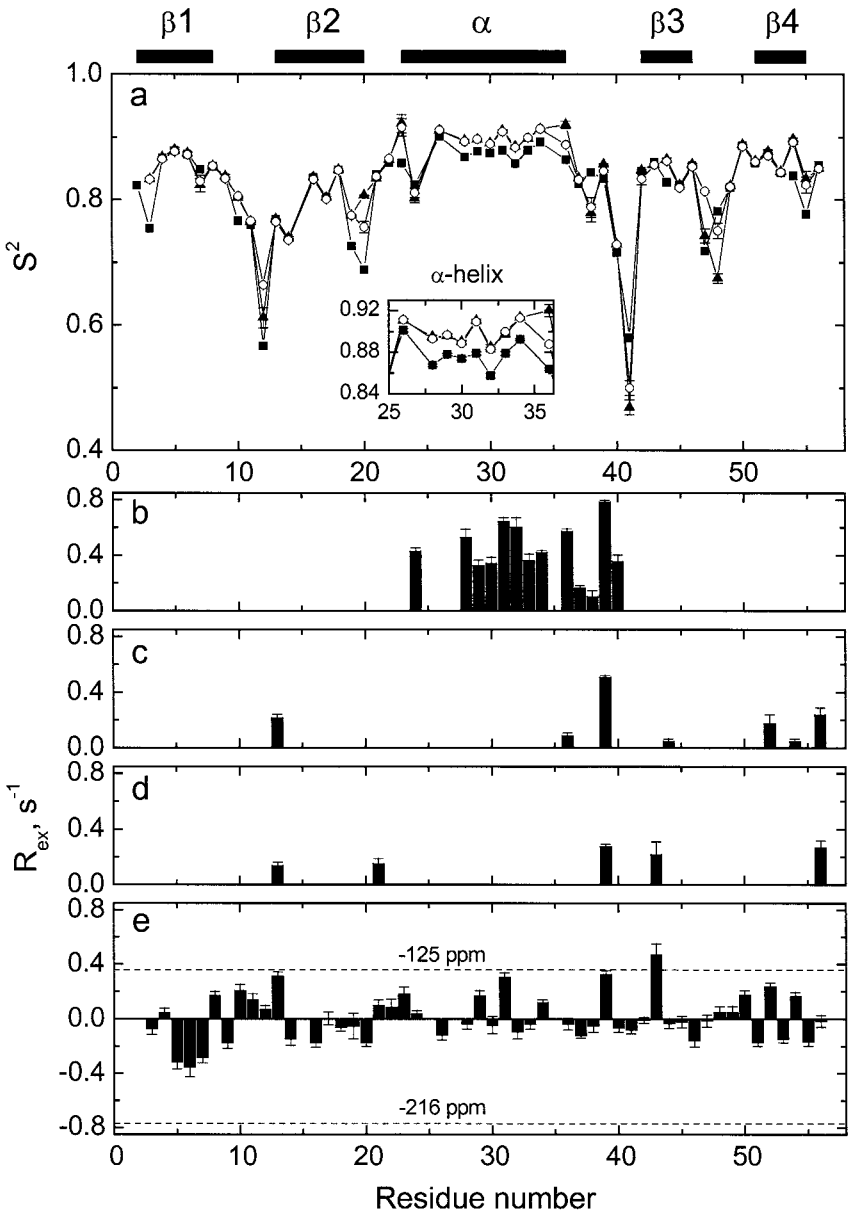

Figure 3. Comparison of the model-free parameters for backbone dynamics in GB3, determined using the three models of the overall tumbling. (a) Squared-order parameters for isotropic (solid squares), axially-symmetric (open circles) and anisotropic (solid triangles) models. (b–d) depict the R_{ex} contributions to R_2 obtained assuming (b) isotropic, (c) axially symmetric and (d) anisotropic models of overall rotational diffusion. (e) R_{ex} values calculated from the experimental data at 9.4 and 14.1 Tesla using Equation 2 and assuming −160 ppm as an average ^{15}N CSA value. Dashed horizontal lines in **e** indicate the average levels of R_{ex} that one would obtain from Equation 2 for the indicated boundary CSA values. Insert in panel **a** is a blowup of the order parameters in the region of the α-helix, to demonstrate the similarities and the differences in order parameters for the three models. The horizontal bars on the top of (a) indicate the elements of secondary structure.

The other R_{ex} predictions of the anisotropic models, for Asp[36], Thr[44], Phe[52] and Val[54] (axially symmetric) and Val[21], Trp[43] (fully anisotropic) are not consistent between these two models nor with the isotropic model. Most of these R_{ex} values are too small (e.g. less than 0.1 s^{-1} for Asp[36], Thr[44], Val[54] and $<$ 0.17 s^{-1} for Val[21], Phe[52]) to indicate real conformational exchange motion and probably represent errors in model selection.

Unlike the isotropic model which is essentially structure-independent, these anisotropic analyses all rely on the information about protein structure and, therefore, could be biased. This seems particularly important for flexible regions of the protein, where crystal structure might provide a snapshot rather than a representative orientation in solution, while a limited number (typically ~20) of structures in the NMR ensemble might not provide proper conformational sampling. In addition, the results of model-free analysis could be biased by the underlying assumptions about the spectral density function and/or by the model-selection procedure. Therefore independent validation of these predictions is required based on methods that do not directly require the knowledge of protein structure or any assumptions about models of motion.

Identification of conformational exchange contributions from cross-correlation measurements

An example of such a model-independent approach is considered here, based on the comparison of R_2 values with the transverse ^{15}N CSA/dipolar cross-correlation rates, η_{xy}. Both η_{xy} and R_2' depend on the same combination of spectral densities (Fushman and Cowburn, 1998a; Fushman et al., 1998), but unlike R_2', η_{xy} contains no contribution from conformational exchange. In the absence of conformational exchange, η_{xy} should scale linearly with R_2', with the proportionality coefficient depending only on parameters reflecting local environment of the ^{15}N nucleus: the NH bond length and the magnitude and orientation of the CSA tensor. Therefore, deviations from linearity of η_{xy} versus R_2' can be used to identify those sites involved in conformational exchange. As pointed out in (Fushman and Cowburn, 1998a), this analysis does not require, hence is not biased by, any information on the protein structure, shape, tumbling rates, or preferred axes of rotation.

Figure 4 illustrates the linear relationship between η_{xy} and R_2' for protein G. Deviations of the data points

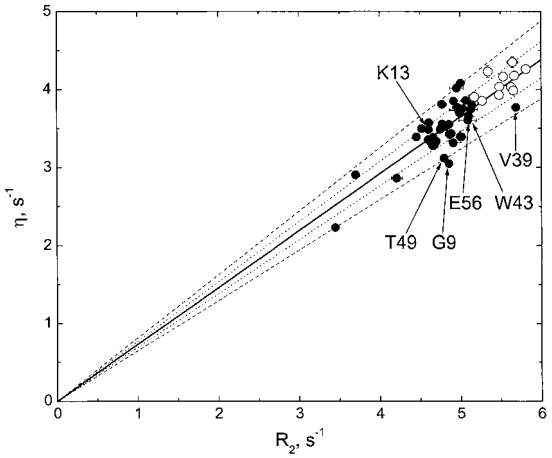

Figure 4. Linear correlation between experimental values of η_{xy} and R_2'. Residues in the α-helix are shown as open circles, while the rest of the backbone amides are represented by solid circles. The fit line (solid) corresponds to a CSA of −160 ppm assuming a β angle of 20° and r_{NH} = 1.02 Å, in excellent agreement with the average values for these parameters reported earlier for ubiquitin (Fushman et al., 1998, 1999a). Similar values were measured in solid state NMR studies of short peptides (e.g., Oas et al., 1987; Hiyama et al., 1988; Shoji et al., 1989). The dashed lines represent the range of ^{15}N CSA values (from −216 ppm to −125 ppm) observed in ubiquitin (here we assumed β=20^o) while the dotted lines correspond to variations in β (20±5°) for CSA = −160 ppm. Note that all helix residues fall within region delimited by boundaries in variations in β and CSA and show no systematic shift to the right of the fit line, indicating that they are not involved in conformational exchange. The positions of Lys[13], Val[39], Trp[43] and Glu[56] (predicted conformational exchange in one or both of the anisotropic models) are indicated. Of these residues, only Val[39] shows a significant shift to the right of the fit line, though it remains within the bounds of variations in CSA measured in ubiquitin. Also indicated are positions of Gly[9] and Thr[49] that, together with Val[39], are the most right-shifted residues.

from the average line may represent conformational exchange, and/or local variations in the ^{15}N CSA and the angle β between the CSA and dipolar tensors (Fushman and Cowburn, 1998a). While site-specific variations in CSA and/or β will cause the data to be distributed on both sides of the average line, the R_{ex} contribution will increase R_2 but not η_{xy} and therefore is expected to result in a horizontal shift of the data to the right.

The data points representing residues in the α-helix all lie to the left or within the error bars from the average line (Figure 4). Since none of these residues is shifted appreciably to the right, we conclude that there is not conformational exchange in the helix. This also suggests that the isotropic tumbling model is inadequate in the case of GB3, and more complicated, anisotopic rotational models are required for data ana-

lysis. Residues that show a noticeable right shift, such as Gly[9], Val[39] and Thr[49], are possible candidates for conformational exchange, though the presence of a small shift alone is not a sufficient condition for determination of conformational exchange as it may be due to residue-specific variations in ^{15}N CSA or β or some combination of these effects.

In order to remove the uncertainty associated with the site-specific variations in the magnitude and orientation of the ^{15}N CSA tensor, we also compared the ratio, η_{xy}/η_z, of the transverse and longitudinal cross-correlation rates with that for the corresponding relaxation rates, R'_2/R'_1. As shown in Kroenke et al. (1998), in the absence of conformational exchange, the two ratios are equal within experimental errors. Therefore, such a comparison can be used as an indicator of the presence of conformational exchange which will increase R'_2/R'_1 but should not affect η_{xy}/η_z. The values of η_{xy}/η_z measured in GB3 agree well with the observed behavior of R'_2/R'_1, the ratio of the two is 1.02 ± 0.03 (Supporting Information). Moreover, the measured values of R'_2 are in good agreement with their 'exchange-free' estimates $R'_{2\text{free}} = (\eta_{xy}/\eta_z)R'_1$; the correlation coefficient between the two is $r = 0.96$ (0.97 if Val[39] is excluded). The comparison of these parameters further supports the conclusion that the elevated values of R_2 (and R'_2/R'_1) in the α-helix are due to rotational anisotropy and not to conformational exchange.

The longitudinal ^{15}N CSA/dipolar cross-correlation rates were measured here in a fully protonated protein, where they could be affected by cross-relaxation with remote protons (Wang et al., 2000). The observed quantitative agreement between the derived η_z values and the rest of relaxation data is somewhat surprising, and could be due to relatively short duration of the relaxation delays. Further studies of this issue are currently in progress.

Identification of conformational exchange contributions from the field dependence of ^{15}N relaxation rates

Another model-independent method for differentiating between conformational exchange and the effects of overall rotational diffusion relies on the field dependence of the R_{ex} terms ($R_{\text{ex}} \propto B_0^2$) in R_2. It is convenient to combine the available ^{15}N relaxation parameters in the following form (Fushman et al., 1999a, Camarero et al., 2001):

$$\begin{aligned} R_J \;\equiv\; & 2R_2 - R_1\left(1 - 0.91\left|\gamma_{\text{N}}/\gamma_{\text{H}}\right|(1-\text{NOE})\right) \\ =\; & 4d^2J(0) + 2\omega_{\text{N}}^2\left[\left(R_{\text{ex}}/\omega_{\text{N}}^2\right)\right. \\ & \left. + 2(\text{CSA}/3)^2J(0)\right], \end{aligned} \tag{1}$$

where $J(0)$ is the spectral density at zero frequency, $d = -(\mu_0/(4\pi))\gamma_{\text{H}}\gamma_{\text{N}}h/(4\pi r_{\text{HN}}^3)$ is the dipolar term, γ_{H} and γ_N are the gyromagnetic ratios for ^{1}H and ^{15}N, r_{HN} is the internuclear distance, and $\omega_{\text{N}} = \gamma_{\text{N}}B_0$ is the Larmor frequency of the ^{15}N nuclear magnetic moment. The field-independent terms, $4d^2J(0)$ and $[(R_{\text{ex}}/\omega_{\text{N}}^2) + 2(\text{CSA}/3)^2J(0)]$, can be determined as the offset and slope, respectively, in the ω^2-dependence of R_J, using relaxation measurements at multiple fields. As pointed out in (Fushman et al., 1999a), this multiple-field method alone does not allow separate determination of the R_{ex} and CSA terms. However, it provides a direct relationship between these quantities, independent of any assumption about the overall or local motion, and therefore allows validation of the predictions of the model-free analysis. For example, for the data measured at two fields, indicated below by the subscripts '1' and '2', simple algebra gives:

$$\begin{aligned} R_{\text{ex}} \;=\; & 0.5\omega_{\text{N}}^2\left\{R_{\text{J}_1}\left[1 + \omega_{\text{N}_2}^2(\text{CSA}/3d)^2\right]\right. \\ & \left. - R_{\text{J}_2}\left[1 + \omega_{\text{N}_1}^2(\text{CSA}/3d)^2\right]\right\}\Big/ \\ & \left(\omega_{\text{N}_1}^2 - \omega_{\text{N}_2}^2\right). \end{aligned} \tag{2}$$

This equation allows determination of the R_{ex} term if the ^{15}N CSA for a given group is known. In the absence of information about site-specific ^{15}N CSA in GB3, it is impossible to use this equation to accurately determine R_{ex}. However, since a uniform ^{15}N CSA value was assumed for the model-free analysis, Equation 2 can be used to verify the predicted R_{ex} values. Figure 3e depicts the R_{ex} term derived from Equation 2 for an average ^{15}N CSA of −160 ppm. The figure also indicates the expected range of R_{ex} variations, assuming the range of ^{15}N CSA values in GB3 is similar to that observed in ubiqutin (Fushman et al., 1998, 1999a), as suggested by Figure 4.

Comparison of these R_{ex} values with the model-free results (Figures 3b–d) for various overall models described in the previous sections suggests that the isotropic model clearly gives false values of R_{ex} for all residues in the region of Ala[23]-Asp[40], except Val[39]. As mentioned above, all overall models predicted conformational exchange contribution for Val[39]. A R_{ex} value slightly above the 'noise' level, cf. Figure 3e, is obtained from Equation 2 for Lys[13], consistent with

the predictions from both anisotropic models. As mentioned above, these R_{ex} contributions are small and hold only for 2/3 of the NMR structures, so whether these are indications of true conformational exchange remains to be investigated. A R_{ex} term also derived from Equation 2 for Trp[43] seems to support the prediction from the fully anisotropic model (Figure 3d). This latter prediction, however, is probably not real, as it holds only for 3 out of the 24 NMR structures.

Note that, like the model-independent approaches presented in the previous section, the analysis based on Equation 2 does not require any information on protein structure or dynamics, and therefore is not biased by any assumption about the structure of protein molecule or its diffusion tensor.

Finally, we also conducted relaxation-compensated CPMG measurements (Loria et al., 1999) to investigate if there are any conformational exchange motions on a slower timescale, up to 8 ms. The data (not shown) indicate no conformational exchange at these timescales for any backbone amides in the GB3 domain.

Explanation of the observed behavior of ^{15}N relaxation data

The analysis presented above solves the issue of apparent conformational exchange contribution versus the effect of rotational anisotropy. However, the question that remains to be addressed is why the increase in R_2 in the residues belonging to the α-helix is not accompanied by a concomitant decrease in R_1. The answer to this question is in the combination of (1) a higher rigidity (increased order parameters) in the α-helix compared to the rest of the backbone and (2) the small size (hence fast overall tumbling) of the protein. While the former is obvious from the elevated heteronuclear NOE values in the helix (Figure 2) and is supported by the results of the model-free analysis for all overall diffusion models (Figure 3), the latter might seem less obvious and requires additional discussion.

The rates of ^{15}N longitudinal and transverse relaxation can be represented as

$$R_1 = 3(d^2 + c^2)J(\omega_N) + 7d^2J(\omega_H);$$

$$R_2 = 0.5R_1 + 2(d^2 + c^2)J(0) + 3d^2J(\omega_H);$$

where $c = -\omega_N \mathrm{CSA}/3$. The difference between R_1 and R_2 in their dependence on the NH vector orientation then stems from the difference between $J(0)$ and $J(\omega_N)$. The high-frequency components, $J(\omega_H)$, are not important for the discussion here, because (A) in proteins they are usually smaller than the lower frequency components and (B) they contribute to both R_1 and R_2. To illustrate the difference between the orientation dependence of $J(0)$ and $J(\omega_N)$ it is convenient to use the concept of local or effective diffusion tensor (Bruschweiler et al., 1991; Lee et al., 1997; Ghose et al., 2001), where the correlation time of the overall tumbling experienced by a NH vector, $\tau_{ceff} = 1/6D_{eff}$, depends on its orientation with respect to the diffusion tensor axes. For example, for the NH bond oriented along the x-, y- or z-axis of the tensor, τ_{eff} can be approximated as

$$\frac{1}{3\left(D_z + D_y\right)}, \quad \frac{1}{3\left(D_z + D_x\right)}, \quad \text{or} \quad \frac{1}{3\left(D_x + D_y\right)},$$

respectively.

For protein core residues with restricted local dynamics on a subnanosecond time scale the spectral density function can be approximated as $J(\omega) \approx S^2\tau_{eff}/(1+\omega^2\tau_{eff}^2)$. For a large protein, with $\omega_N\tau_{eff} \gg 1$, this gives

$$R_1 \approx 3(d^2 + c^2)\frac{S^2}{\omega_N^2\tau_{eff}}$$

and

$$\begin{aligned} R_2 &\approx (d^2 + c^2)\left\{2S^2\tau_{eff} + 1.5\frac{S^2}{\omega_N^2\tau_{eff}}\right\} \\ &\approx 2(d^2 + c^2)\ S^2\tau_{eff}, \end{aligned}$$

hence the inverse dependence of the transverse and longitudinal relaxation rates on τ_{eff} (and thus on the orientation of N-H vectors with respect to the diffusion tensor axes) typically observed in proteins. Note that in this case the $J(\omega_N)$-contribution to R_2 becomes negligible, so $J(0)$ is the dominant term.

For a smaller protein that rotates faster in solution and hence has a smaller rotational correlation time, the product $\omega_N\tau_{eff}$ can be of the order or less than 1. For $\omega_N\tau_{eff} \approx 1$, $J(\omega_N)$ as a function of τ_{eff} is near its maximum where it very slowly changes with τ_{eff}, while $J(0)$ remains linear in τ_{eff}. Therefore, in this regime, R_1 should be significantly less sensitive than R_2 to the orientation of the NH bond. This also suggests that variations in the rate of longitudinal relaxation will mainly reflect variations in the local backbone dynamics and in ^{15}N CSA. For even smaller molecules, $\omega_N\tau_{eff} \ll 1$, and both $J(0)$ and $J(\omega_N)$ scale linearly with τ_{eff}. As a result, R_1 will depend on the NH bond orientation in approximately same way as R_2.

Due to the relatively fast tumbling ($\tau_c = 3.34$ ns) under the experimental conditions, the GB3 domain falls into the regime of $\omega_N\tau_{eff} \approx 1$: the τ_{eff} values range from 3.01 to 3.75 ns ($\omega_N\tau_{eff}$ from 1.15 to 1.43) depending on the NH bond orientation. Given the NH vectors in the α-helix are almost parallel and those in the rest of the protein core (β-sheet) are almost orthogonal to the z-axis of the diffusion tensor, these numbers result in a 14% increase in R_2 and a 5% decrease in R_1 in the helix compared to the rest of the protein. The corresponding numbers from a more accurate calculation assuming a 23° angle between the helix and the diffusion tensor axis are 12% and 4%. These calculations consider only orientation dependence of the relaxation rates due to anisotropy of the overall tumbling and do not include site-specific variations in local dynamics or ^{15}N CSA. Taking into account ~7% higher S^2 values in the helix (Figure 3a), this will result in a 2–3% total increase in the R_1. This is in excellent agreement with the experimental data indicating a 2% increase in R_1 in the α-helix compared with the β-strands.

It is worth mentioning that because in GB3 the rates of ^{15}N longitudinal relaxation are relatively insensitive to NH bond orientation, they correlate well with the derived order parameters. For example, the correlation coefficient between S^2 derived using axially symmetric model and the measured R_1 values is 0.95, whereas a weaker correlation is observed between S^2 and R_2 (0.86) or NOE (0.88).

Comparison with predictions from hydrodynamic models

Theoretical prediction of the rotational properties of proteins in solution is complex, largely because it has to account for the unknown size and shape of the hydration shell formed by nearby water molecules moving together with the tumbling protein molecule. For example, a simple hydrodynamic calculation (above) based on the size of a 'dry' protein molecule results in a reasonable estimate (within 6%) of the anisotropy of the tensor but significantly (by 30–40%) overestimates the rate of molecular rotation. A detailed theoretical analysis should consider specific interactions between water molecules and protein atoms and the friction effects due to the roughness of the protein surface (Fushman, 1990).

Having experimental data for the rotational diffusion tensor of the protein, we can now test if current theoretical models are capable of reproducing these results. Here we focus on two characteristics of the diffusion tensor: its anisotropy and the overall correlation time. We select these parameters because of the opposite character of their dependence on the size of the hydration shell: adding a layer of water molecules will increase τ_c (as the rotating body is now larger) and decrease the $D_{||}/D_{\perp}$ (as the hydration shell enclosed protein is more rounded than the protein alone). Note that, in contrast to τ_c, the anisotropy ($D_{||}/D_{\perp}$) is a dimensionless quantity, which is size-independent and should reflect only the shape of the molecule including the hydration shell. Therefore a simultaneous comparison of the predictions for both characteristics of the tensor could provide insights into the optimal settings for theoretical hydrodynamic models.

The so-called 'bead model' for prediction of the hydrodynamic properties of molecules approximates protein by a series of beads (de la Torre et al., 1994) placed at the coordinates of heavy atoms and with the bead size representing the average atomic radius. First we considered a 'dry protein'. For the B3 domain of protein G we could reproduce the experimentally obtained value of τ_c for an atomic radius of 1.45 Å, and the experimentally obtained value of $D_{||}/D_{\perp}$ for a radius of 1.1 Å. Theoretically, one average atomic radius should reproduce both experimental parameters of overall rotational diffusion. Therefore we conclude that the 'dry protein' model is not adequate. We then included hydration shells of increasing thickness (0–5 Å) to the protein bead model to test if this could reproduce the values of both experimental parameters ($D_{||}/D_{\perp}$ and τ_c) for one bead size and one shell thickness. For these calculations, the protein molecule was 'soaked' in water using a 5 Å shell following standard procedure in Insight (MSI), and then only those waters within a given distance (shell thickness) from the protein atoms were considered. It turns out that several combinations of bead size and hydration shell thickness are consistent with the experimental values (see Figure 5a), given the experimental uncertainties. The optimal bead sizes ranged from 0.8 to 1.2 Å and the corresponding values of the shell thickness from 1.2 to 1.5 Å. The latter values are somewhat smaller than those typically used in hydrodynamic calculations.

Another, more recent method for calculating surface effects of molecules in solution, uses a strategy known as 'shell modeling' (García de la Torre et al., 2000), where the hydration effects are represented by a shell covering the surface of the protein. This model is characterized by a single parameter a that represents the sum of the thickness of the hydration shell

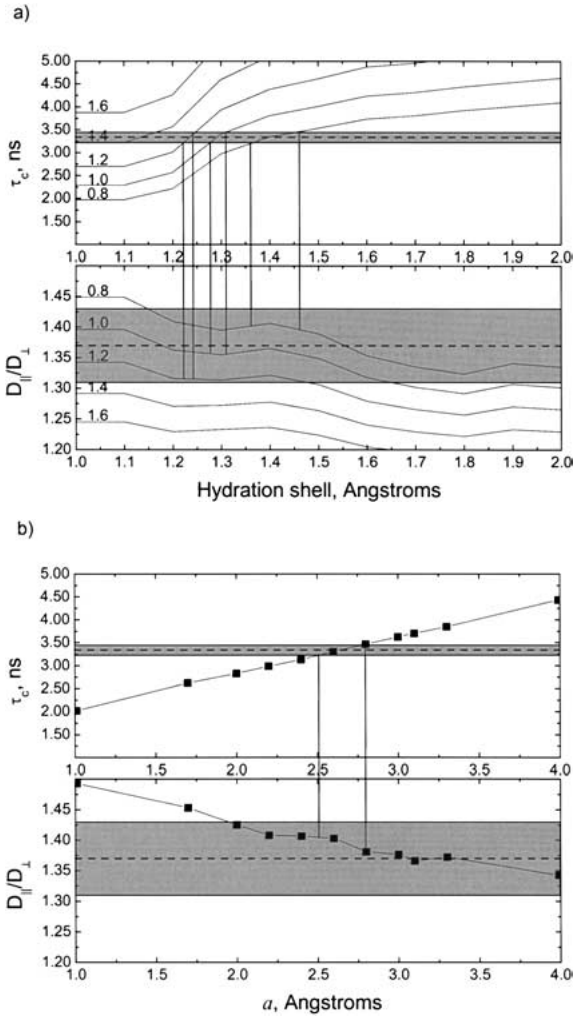

Figure 5. Comparison of the measured characteristics, τ_c and $D_{||}/D_{\perp}$, of the diffusion tensor with the results of hydrodynamic calculations. (a) 'Bead model': Dependence of the hydration shell thickness for various atom 'bead' sizes, indicated by the corresponding numbers for each line. (b) 'Shell model' (HYDRONMR): Dependence on the parameter a (average van der Waals radius of the atoms in the molecule plus the thickness of the hydration shell). The dashed lines represent the experimental values of the diffusion tensor characteristics derived for the axially symmetric model, while the shaded areas represent their 68.3%-confidence region. The vertical bars in (a) mark the regions which are inside the experimental errors for both measured parameters ($D_{||}/D_{\perp}$ and τ_c) for a particular bead size. Similar bars in (b) indicate the range of shell thickness that is consistent with both experimental parameters.

and the average atomic van der Waals radius in the molecule. For the B3 domain of protein G we were able to reproduce the experimentally obtained values for both τ_c and $D_{||}/D_{\perp}$ for an a between 2.5 Å and 2.8 Å (Figure 5b). As shown in Table 1, both the principal values and the orientation of the calculated diffusion tensor are in remarkable agreement with the experimental data. Assuming an average atomic van der Walls radius of a heavy atom in the protein is about 1.5 Å, the hydration shell should have a thickness of between 1.0 Å and 1.3 Å. This is generally consistent with the results of the bead model, where the hydration shell thickness was calculated to be between 1.2 Å and 1.5 Å.

Values of parameter a between 2.5 Å and 2.8 Å are consistent with the results obtained by García de la Torre et al. (2000) who calculated rotational diffusion tensors for a variety of a values for 15 proteins covering a range of molecular weights from 2.93 to 26.7 kDa. They found that in most cases experimental values of τ_c were reproduced with values of a between 2 Å and 4 Å.

We have also computed the rhombicity factor, $1.5(D_y - D_x)/[D_z - 0.5(D_x + D_y)]$ for the various hydration shell models considered here. The value for the dry protein was 0.16. For a hydrated protein the derived values of the factor range from 0.13 to 0.23 for the bead model calculations with various bead sizes and shell thickness, and from 0.16 to 0.20 for the shell model. The parameters of the models were the same as in Figure 5. Our hydrodynamic calculations show that the rhombicity factor is less sensitive to the size of the hydration shell than τ_c. The results of our analysis indicate that the rotational properties of GB3 slightly deviate from ideal axial symmetry. The calculated rhombicity of the diffusion tensor is small and agrees with the measured value (Table 1) within the experimental errors.

Conclusions

Our analysis of ^{15}N relaxation data for the B3 domain of protein G, a 56 a.a. protein with intermediate rotational anisotropy $D_{||}/D_{\perp} = 1.4$, shows that the isotropic and anisotropic models of the overall tumbling result in markedly different pictures of local motion. Both axially symmetric and fully anisotropic models for the overall motion fit the experimental data significantly better than does the isotropic model. The diffusion tensor of the molecule is close to axially

symmetric, with its longitudinal axis being almost parallel to the axis of the helix, in excellent agreement with theoretical predictions from hydrodynamic calculations. This explains the elevated R_2 values observed in the α-helix that could otherwise be interpreted as indications of the conformational exchange motions when isotropic tumbling is assumed. Moreover, because of the small size of the protein, its tumbling rate falls into the range ($\tau_c\omega_N \sim 1$) where R_1 is practically insensitive to NH bond orientation and mainly reflects variations in the order parameter. Combined with slightly higher backbone rigidity in the α-helix, this explains why, contrary to the common expectations for anisotropic diffusion, an increase in R_2 in the α-helix is not accompanied by a concomitant decrease in R_1. If the small size (fast tumbling) of the protein is not taken into consideration, the observed behavior of R_2 and R_1 could be interpreted as an indication of the presence of conformational exchange.

Since the results of the anisotropic models could be biased by the available structural information, additional, model-independent methods are required which do not rely on the knowledge of protein structure or assumptions about its dynamics in order to distinguish the correct picture of motion. Two such methods are applied here to differentiate between the effects of conformational exchange and rotational anisotropy: a comparison of the CSA/dipolar cross-correlation rates (η_{xy}, η_z) with relaxation rates (R_2, R_1) and the estimation of R_{ex} terms from ^{15}N relaxation data at two fields. Both methods are (1) sensitive to conformational exchange, (2) do not require knowledge of protein structure or (3) any assumption about the spectral density function, and therefore can be used to either identify potential sites for conformational exchange or verify the absence thereof. These analyses provide no indication of conformational exchange in the helix, consistent with the predictions from anisotropic models. A more accurate analysis including site-specific values of ^{15}N CSA is currently in progress.

Acknowledgements

We thank Dr Ad Bax for providing us with the protein sample, Dr Ben Ramirez for NMR signal assignments, and Dr Olivier Walker for help with fully anisotropic analysis of rotational diffusion. Supported by NIH grant GM65334-01 to D.F. D.F. also acknowledges travel grant from the Faculty of Sciences University of Florence and is grateful to Prof Ivano Bertini for NMR measurement time.

References

Achari, A., Hale, S.P., Howard, A.J., Clore, G.M., Gronenborn, A.M., Hardman, K.D. and Whitlow, M. (1992) *Biochemistry*, **31**, 10449–10457.

Akke, M. and Palmer, III, A.G. (1996) *J. Am. Chem. Soc.*, **118**, 911–912.

Barchi, Jr., J.J., Grasberger, B., Gronenborn, A.M. and Clore, G.M. (1994) *Protein Sci.*, **3**, 15–21.

Blackledge, M., Cordier, F., Dosset, P. and Marion, D. (1998) *J. Am. Chem. Soc.*, **120**, 4538–4539.

Bruschweiler, R., Blackledge, M. and Ernst, R.R. (1991) *J. Biomol. NMR*, **1**, 3–11.

Camarero, J.A., Fushman, D., Sato, S., Giriat, I., Cowburn, D., Raleigh, D.P. and Muir, T.W. (2001) *J. Mol. Biol.*, **308**, 1045–1062.

Clore, G.M., Driscoll, P.C., Wingfield, P.T. and Gronenborn, A.M. (1990a) *Biochemistry*, **29**, 7387–7401.

Clore, G.M., Szabo, A., Bax, A., Kay, L.E., Driscoll, P.C. and Gronenborn, A.M. (1990b) *J. Am. Chem. Soc.*, **112**, 4989–4936.

Copie, V., Tomita, Y., Akiyama, S.K., Aota, S., Yamada, K.M., Venable, R.M., Pastor, R.W., Krueger, S. and Torchia, D.A. (1998) *J. Mol. Biol.*, **277**, 663–682.

de la Torre, J.G., Navarro, S., Martinez, M.C.L., Diaz, F.G. and Cascales, J.J.L. (1994) *Biophys. J.*, **67**, 530–531.

Derrick, J.P. and Wigley, D.B. (1992) *Nature*, **359**, 752–754.

Derrick, J.P. and Wigley, D.B. (1994) *J. Mol. Biol.*, **243**, 906–918.

Derrick, J.P., Wigley, D.B., Lian, L.Y., Sutcliffe, M.J., Yang, J.C., Dawson, P.D. and Roberts, G.C. (1993) *Biochem. Soc. Trans.*, **21**, 333S.

Dosset, P., Hus, J.C., Blackledge, M. and Marion, D. (2000) *J. Biomol. NMR*, **16**, 23–28.

Eisenmesser, E.Z., Bosco, D.A., Akke, M. and Kern, D. (2002) *Science*, **295**, 1520–1523.

Farrow, N.A., Muhandiram, R., Singer, A.U., Pascal, S.M., Kay, C.M., Gish, G., Shoelson, S.E., Pawson, T., Forman-Kay, J.D. and Kay, L.E. (1994) *Biochemistry*, **33**, 5984–6003.

Fushman, D. (1990) *J. Biomol. Struct. Dyn.*, **7**, 1333–1344.

Fushman, D. (2002) In *BioNMR in Drug Research*, Zerbe, O. (Ed.), Wiley-VCH, New York, NY, pp. 283–308.

Fushman, D. and Cowburn, D. (1998a) *J. Am. Chem. Soc.*, **120**, 7109–7110.

Fushman, D. and Cowburn, D. (1998b) In *Structure, Motion, Interaction and Expression of Biological Macromolecules*, Sarma, R. and Sarma, M. (Eds.), Adenine Press, Albany, NY, pp. 63–77.

Fushman, D. and Cowburn, D. (2002) In *Protein NMR for the Millenium* (*Biological Magnetic Resonance*, Vol 20), Krishna N.R. and Berliner, L.J. (Eds.), Kluwer Academic Publishers, New York, NY, pp. 53–78.

Fushman, D., Cahill, S. and Cowburn, D. (1997) *J. Mol. Biol.*, **266**, 173–194.

Fushman, D., Tjandra, N. and Cowburn, D. (1998) *J. Am. Chem. Soc.*, **120**, 10947–10952.

Fushman, D., Tjandra, N. and Cowburn, D. (1999a) *J. Am. Chem. Soc.*, **121**, 8577–8582.

Fushman, D., Xu, R. and Cowburn, D. (1999b) *Biochemistry*, **38**, 10225–10230.

Gallagher, T., Alexander, P., Bryan, P. and Gilliland, G.L. (1994) *Biochemistry*, **33**, 4721–4729.

García de la Torre, J., Huertas, M.L. and Carrasco, B. (2000) *J. Magn. Reson.*, **B147**, 138–146.
Ghose, R., Fushman, D. and Cowburn, D. (2001) *J. Magn. Reson.*, **149**, 214–217.
Gronenborn, A.M., Filpula, D.R., Essig, N.Z., Achari, A., Whitlow, M., Wingfield, P.T. and Clore, G.M. (1991) *Science*, **253**, 657–661.
Grzesiek, S. and Bax, A. (1993) *J. Am. Chem. Soc.*, **115**, 12593–12594.
Hall, J.B., Dayie, K.T. and Fushman, D. (2003) *J. Biomol. NMR*, **26**, 181–186.
Hiyama, Y., Niu, C., Silverton, J., Bavoso, A. and Torchia, D. (1988) *J. Amer. Chem. Soc.*, **110**, 2378–2383.
Ishima, R., Wingfield, P., Stahl, S., Kaufman, J. and Torchia, D.A. (1998) *J. Am. Chem. Soc.*, **120**, 10534–10542.
Jones, J.A. (1997) *J. Magn. Reson.*, **126**, 283–286.
Kay, L.E., Torchia, D.A. and Bax, A. (1989) *Biochemistry*, **28**, 8972–8979.
Koradi, R., Billeter, M. and Wüthrich, K. (1996) *J. Mol. Graph.*, **14**, 51–55.
Kroenke, C.D., Loria, J.P., Lee, L.K., Rance, M. and Palmer, A.G.I. (1998) *J. Am. Chem. Soc.*, **120**, 7905–7915.
Lee, L.K., Rance, M., Chazin, W.J. and Palmer, III, A.G. (1997) *J. Biomol. NMR*, **9**, 287–298.
Lian, L.Y., Derrick, J.P., Sutcliffe, M.J., Yang, J.C. and Roberts, G.C. (1992) *J. Mol. Biol.*, **228**, 1219–1234.
Lipari, G. and Szabo, A. (1982) *J. Am. Chem. Soc.*, **104**, 4559–4570.
Loria, J.P., Rance, M. and Palmer, A.G.I. (1999) *J. Am. Chem. Soc.*, **121**, 2331–2332.
Luginbuhl, P., Pervushin, K.V., Iwai, H. and Wüthrich, K. (1997) *Biochemistry*, **36**, 7305–7312.
Mandel, A.M., Akke, M. and Palmer, III, A.G. (1995) *J. Mol. Biol.*, **246**, 144–163.
Oas, T.G., Hartzell, C.J., Dahlquist, F.W. and Drobny, G.P. (1987) *J. Am. Chem. Soc.*, **109**, 5962–5966.
Orekhov, V., Pervushin, K.V. and Arseniev, A.S. (1994) *Eur. J. Biochem.*, **219**, 887–896.
Ottiger, M., Delaglio, F. and Bax, A. (1998) *J. Magn. Reson.*, **131**, 373–378.
Palmer, III, A.G. (1997) *Curr. Opin. Struct. Biol.*, **7**, 732–737.
Palmer, A.G., Williams, J. and McDermott, A. (1996) *J. Phys. Chem.*, **100**, 13293–13310.
Schurr, J.M., Babcock, H.P. and Fujimoto, B.S. (1994) *J. Magn. Reson.*, **B105**, 211–224.
Shoji, A., Ozaki, T., Fujito, T., Deguchi, K., Ando, S. and Ando, I. (1989) *Macromolecules*, **22**, 2860–2863.
Szyperski, T., Luginbuhl, P., Otting, G., Guntert, P. and Wüthrich, K. (1993) *J. Biomol. NMR*, **3**, 151–164.
Tillett, M.L., Blackledge, M.J., Derrick, J.P., Lian, L.Y. and Norwood, T.J. (2000) *Prot. Sci.*, **9**, 1210–1216.
Tirado, M.M. and de la Torre, J.G. (1980) *J. Chem. Phys.*, **73**, 1986–1993.
Tjandra, N., Feller, S.E., Pastor, R.W. and Bax, A. (1995) *J. Am. Chem. Soc.*, **117**, 12562–12566.
Tjandra, N., Szabo, A. and Bax, A. (1996a) *J. Am. Chem. Soc.*, **118**, 6986–6991.
Tjandra, N., Wingfield, P., Stahl, S. and Bax, A. (1996b) *J. Biomol. NMR*, **8**, 273–284.
Wang, L., Kurochkin, A.V. and Zuiderweg, E.R. (2000) *J. Magn. Reson.*, **144**, 175–185.